Food Analytical Methods
https://doi.org/10.1007/s12161-022-02409-w

Individual and Simultaneous Electrochemical Detection of Bisphenol A and Bisphenol S in Food Samples Using Triethylenetetramine Functionalized Multi-Walled Carbon Nanotubes

Maşide Çakıcı[1] · Asiye Aslıhan Avan[2] · Hayati Filik[2] · Ece Kök Yetimoğlu[3]

Received: 19 June 2022 / Accepted: 20 September 2022

Abstract
In this concept, multi-walled carbon nanotubes (MWCNTs) were functionalized by triethylenetetramine (TETA-MWCNTs), and the as-synthesized TETA-MWCNT materials were utilized for the simultaneous voltammetric detection of bisphenol A (BPA) and bisphenol S (BPS). The voltammetric behaviors were tested by cyclic voltammetry (CV) and square-wave voltammetry (SWV). The high-priority experimental parameters have been carefully optimized. The designed sensor exhibited exceptional electrocatalytic activity toward the oxidation of BPA and BPS and provided two well-separate oxidation peaks enough to quantify BPA and BPS in a binary mixture. The standard curve was linear over the concentration range of 1.0–30 μM for both analytes. The detection limit was estimated to be 0.35 μM and 0.56 μM for BPA and BPS, respectively. The designed voltammetric sensor was successfully applied in simultaneous estimation of BPA and BPS in food samples.

Keywords Bisphenol A · Bisphenol S · Electrochemical sensor · Triethylenetetramine · Carbon nanotubes · Food analysis

Introduction

Bisphenol A (BPA) (2,2-bis(4-hydroxyphenyl) propane) is one of the most famous endocrine-disrupting chemicals (EDCs) (Thoene et al. 2018). Likewise, bisphenol S (BPS) (4, 4′-sulfonyldiphenol, related to its chemical cousin BPA, is an organic compound utilized to make hard plastic products and synthetic fibers. Besides, BPS is more heat-stable and photo-resistant than BPA and therefore replaces BPA (Zhao et al. 2018). Moreover, BPS is a BPA analog in which the dimethyl methylene group are changed by a sulfonyl functional group which can enhance the chemical stability of the molecule. BPS has a lower risk to the environment and human health than BPA but it is not amenable to biodegradation. Numerous studies introduce that BPS retains analog estrogenic action, causes chronic disorders, and exhibits environmental durability (Rao et al. 2018; Zhu et al. 2016). Above all, EDCs are found in numerous everyday materials, including some plastic bottles and containers, metal-canned foods, toys, detergents, cosmetics, and pesticides (Zhang et al. 2018a; Zheng et al. 2018). Both compounds (BPA and BPS) have similar chemical structures which both comprise two hydroxyphenyl groups and are named bisphenol (BP) analogs. Resulting from the universal use of BPs in daily products, a mass of BP leaching from various materials exists in food, environmental medium, and living organisms (Baluka and Rumbeiha 2016; Huang et al. 2018). Except for specific endocrine-disrupting impacts, BPs are suspected to be related to many chronic diseases such as reproductive disorders, cardiovascular diseases, breast cancer, diabetes, obesity, and birth defects (Zhang et al. 2018b). Because of ecological and human health risks, many countries have banned the utilization of various products with BP addition. BP compounds or derivatives can generally co-exist in the same medium (water, food, and so on) and interfere reciprocally in detection and quantification protocol due to their analog chemical structures and attributes (Wang et al. 2017). Therefore, it is needed to improve a

✉ Hayati Filik
filik@istanbul.edu.tr

[1] Department of Chemistry, Institute of Pure and Applied Sciences, Marmara University, Kadıköy, Istanbul 34722, Turkey

[2] Department of Chemistry, Faculty of Engineering, Istanbul University-Cerrahpaşa, 34320 Avcılar, Istanbul, Turkey

[3] Department of Chemistry, Faculty of Arts and Science, Marmara University, Kadıköy, Istanbul 34722, Turkey

Published online: 28 September 2022

rapid, sensitive, and precise analytical concept for the sensing of two target EDCs.

Up to now, instrumental analysis based on the principles of chromatography and mass spectrometry has still been the main method to detect BPA and BPS content in various samples (García-Córcoles et al. 2018; Rocha et al. 2018; Wang et al. 2017). Even though these conventional analytical techniques have advantages of high accuracy and sensitivity, they also require a complex pretreatment process, time-consuming analyses, expensive instruments, special organic solvents, and trained operators. Hence, electrochemical methods are used as a convenient way for the rapid and accurate detection of BPs. In recent years, the electrochemical sensor has shown promising potential for its advantages of simple operation, time-saving, high sensitivity, and portability. BPA and BPS have two phenolic hydroxyl groups, and at a certain potential, the phenolic hydroxyl groups can be oxidized to a quinone. Nanomaterials are considered to be ideal materials for improving the sensitivity and selectivity of electrochemical sensors (Butmee et al. 2019; Canevari et al. 2019).

Various remediation technologies have been developed and reported for the determination of BPA and BPS and other EDCs. BPA and BPS with good electrochemical activity can display two separated oxidation peaks by the voltammetric method (Zheng et al. 2016). However, since EDCs have similar chemical architectures and oftentimes co-exist in the environmental medium, it causes some issues in voltammetric detection. To find a way out of these drawbacks, different efforts have been made to modify electrodes with graphene, carbon nanotubes (CNTs), quantum dots (QDs), metal–organic frameworks (MOFs), Ni-loaded $CdFe_2O_4$, conducting polymer (CP), SiO_2/graphene oxide/Ag nanoparticles, graphite-polyurethane composites, and flexible carbon fiber sheets (Avan and Filik 2018; Baccarin et al. 2020; Campos et al. 2016; de Sá et al. 2020; Ezoji and Rahimnejad 2018; Filik and Avan 2017; Filik et al. 2019; Lu et al. 2016; Mo et al. 2019; Rao et al. 2018; Wang et al. 2015; Yao et al. 2019). To date, only a few electrochemical-based sensors have been reported for the simultaneous sensing of the target EDCs. For example, a platinum (Pt) nanoparticles-functionalized poly(diallyl dimethyl ammonium chloride) (PDDA)-diamond powder (DMP) composite-modified GCE was fabricated for electrochemical sensing of the selective or simultaneous determination of BPA and BPS. DMP is a pure carbon material with an abundant negative charge. It has high chemical and electrochemical properties, as well as strong resistance to high temperature and corrosion. Its electrochemical response can remain stable for a long time. Pt nanoparticles were synthesized in situ on the surface of PDDA-DMP using H_2PtCl_6 as the precursor by reduction of ethylene glycol (Zheng et al. 2016). The differential pulse voltammetry (DPV) in 0.1 M phosphate buffer solution (pH 6.0) has been applied to their simultaneous determination in river water and thermal paper samples using a -COOH functionalized MWCNTs modified GCE (Wang et al. 2018). Compared with conventional materials, covalent organic framework (COFs) have the advantages of large specific surface area, good chemical and thermal stability, π conjugation, tunable porosity, and low density, which make them potentially useful in diverse fields (gas storage, photoconduction, catalysis, and so on). For example, Pang et al. (2020), constructed a highly porous crystalline COF, CTpPa-2-modified GCE for the electrochemical sensing of BPA and BPS. The electrochemical properties of the CTpPa-2/GCE were characterized using galvanostatic charge–discharge, CV, and DPV. The electrochemical responses for BPA and BPS were found to be linear in the concentration ranges of 0.1–50 μM and 0.5–50 μM with detection limits of 0.02 μM and 0.09 μM, respectively. Finally, the three-component composite material AuAgPt-β-cyclodextrin polymer (PCD)-graphene oxide (GO) was properly designed to construct a novel electrochemical sensor for simultaneous BPA and BPS assay (Ye et al. 2019). The response linear ranges for BPA and BPS are from 6 to 4000 nM and 8 –8000 nM with detection limits of 2 nM and 2.67 nM, respectively.

Among the different carbon nanomaterials, carbon nanotubes (CNTs) are slowly attracting attention owing to their ease of synthesis, fluorescent nature, relatively low/non-toxicity, high surface area and functional ability. Carbon nanotubes (MWCNTs or SWCNTs) have been accepted as good candidates to rehabilitate the performance of electrochemical sensors due to their extraordinary chemical, physical, and electrical attributes. Also, CNTs present a large surface area, chemical robustness, and fast electron transfer ability, which are responsible for their prevalence utilized as voltammetric sensing materials (Dubey et al. 2021; Li et al. 2018). Despite their amazing features, CNTs demonstrate very low dispersibility and a high tendency to agglomerate in ordinary polar and non-polar solvents (Li et al. 2019). Procedures to accomplish this difficulty comprise surface modification of CNTs with polymers, small molecules, and biomolecules, incorporation in composite matrices, and doping with external atoms (González et al. 2016; Yang et al. 2019). The modification of CNTs (and other carbon materials) either by physical or chemical treatments, is known to induce new properties or enhance some already existing properties. The surface alteration of CNTs improves the reactivity and solubility and ensures an avenue for further surface alteration of CNTs such as metal deposition, ion adsorption, and functional group reactions. Meanwhile, the surface groups can also serve as linking groups for combining two fragments and further derivatization by chemical interactions with other specific functional groups (Noordadi et al. 2018; Wolski et al. 2017). Previous research reported that the amide or amine functional groups (or derivatives) in functionalized CNTs could attract the protons from electrolyte solution due

to their conjugation (Li et al. 2016a; Shalom et al. 2014; Zheng et al. 2014), and this protonation could be a crucial factor to promote analyte activity. Herewith, amide/amine attached architectures (CNTs, GO, and so on) have a crucial potential for the detection of specific analytes as electrocatalysts because of their proton adsorption ability and electron transfer features. Also, the abovementioned textures can be synthesized with a low cost and simple strategy.

In the current strategy, an electrochemical sensor based on TETA-functionalized MWCNTs has been established for simultaneous monitoring of BPA and BPS. The electrooxidation of both analytes was carefully evaluated by CV and SWV techniques. The TETA-MWCNTs-modified GCE displayed sufficient electrocatalytic performance toward the oxidation of target EDCs. The suggested sensing concept was successfully implemented in real food samples with convincing results.

Material and Methods

Instrumentation and Chemicals

The electrochemical measurements (CV, EIS, and SWV) were made with Gamry series 600 potentiostat/galvanostat. All measurements were recorded using a 10-mL electrochemical cell that has a three-electrode system. The electrodes used were 3.0-mm GCE (modified GCE) as the working electrode, Ag/AgCl (with a 3 M KCl) as the reference electrode, and platinum wire (Pt) as the counter electrode. Before each modification process, the GCE surface has been polished and then rinsed twice with distilled water followed by ethanol to remove encrusted materials on the electrode surface. Fourier transform ınfrared (FTIR) spectra were obtained using a Bruker Vertex 70v FTIR spectrometer (Bruker Optics, Germany). The surface morphology of carbon nanotubes was examined by using a scanning electron microscope (SEM) Zeiss Sigma 300 SEM (Zeiss, Germany). Multi-walled carbon nanotubes (MWCNTs > 95% carbon basis, O.D. × L: 10–20 nm × 20–50 μm) and TETA (purity ≥ 97%) were purchased from Sigma, St. Louis. All chemicals used in the experiments were of reagent grade and were employed as provided without any further separation. In this context, BPA, BPS, N, N-Dimethylformamide (DMF) (≥ 99%), thionyl chloride ($SOCl_2$) (≥ 99%), H_2SO_4 (98%), H_3PO_4 (≥ 85%), HCl (37%), and CH_3COOH were obtained from Sigma-Aldrich. Boric acid (H_3BO_3), HNO_3 (68%), NaOH (Pellets), $K_4[Fe(CN)_6]0.3H_2O$, $K_3[Fe(CN)_6]$, and KCl were obtained from Merck. Britton Robinson buffer (BRB) solution was prepared by mixing 0.1 M each of H_3PO_4, H_3BO_3, and CH_3COOH. A series of BRBs in the pH range of 3.0–7.0 was prepared by the addition of 1 M NaOH. Alumina polishing slurries were provided from Buehler, LL, USA and were employed for polishing the bare GCE surface before the modification process. Distilled water has been used for all voltammetric experiments. BPA and BPS stock solutions (both 2 mM) were prepared by dissolving appropriate amounts in 5 mL of ethanol and then diluted with 50 mL of distilled water.

Synthesis of Functionalized MWCNTs

Initially, the carboxylic acid-functionalized MWCNT nanocomposites were synthesized. The raw-MWCNTs (500 mg) were properly oxidized by a mixture of sulfuric acid and nitric acid (V:V = 3:1, 80 mL) at 70 °C for 6 h to occur -COOH group on the MWCNTs. The carboxylated MWCNTs were then properly filtered (0.4-μm cellulose acetate membrane), after that, the ox-MWCNTs were washed properly with distilled water until the aqueous phase was neutral. For TETA graft MWCNTs, initially, the ox-MWCNTs (~ 400 mg) were carefully mixed with $SOCl_2$ (25 mL) and DMF (10 mL). DMF was also used to disperse the MWCNTs. Subsequently, the dispersed solution was appropriately refluxed at 70 °C for 96 h. After the process was completed, the acyl chloride-MWCNTs (MWCNT-COCl) powder, was reached after filtration and then washed twice with DMF (5 mL) to separate surplus $SOCl_2$ and then dried for 6 h in a vacuum oven at 80 °C. The resulted MWCNT-COCl was reacted with 10 mL of pure TETA (purity ≥ 97% (TETA is a moderately viscous, yellowish liquid) for 48 h at 100 °C and washed sufficiently with ethanol to eliminate excess TETA. Consequently, the obtained products are named TETA-MWCNTs (MWCNT-CO-TETA). Ten milligrams of TETA-MWCNTs were sonicated for about 5 min in 10 mL distilled water (1 mg/mL) to achieve a homogenous mixture and this dispersion was used for electrode modification.

Treatment of Samples

Commercial food samples, such as drinking water, milk, cola, and juice, were provided from local markets. The standard addition protocol was performed by spiking samples with known amounts of the target EDCs. On the other hand, milk sample preparation was carried out using a protein precipitation extraction strategy. Each sample (5 mL milk) was properly extracted twice with 5.0 mL ethanol under ultrasound for 15 min, after that, centrifuged for 10 min at 4000 rpm. The upper aqueous phase was carefully transferred to a new tube by pipetting, and the obtained protein-free milk was collected and used for further analysis.

Modification of GCE

In the beginning, the naked GCE was properly brightened to a mirror surface with alumina slurry (0.3 µm) and washed twice with distilled water and then, the GCE was sonicated in ethanol and distilled water (each for 5 min) and dried. After drying at surrounding temperature, 5 µL of TETA-MWCNT (1 mg/mL) architectures were evenly dropped onto the brightened GCE surface and it was adequately dried at surrounding temperature. For comparison, the same strategy was exploited to construct MWCNTs-modified GCE.

Electrochemical Measurement Process

Initially, the modified electrode was first rinsed with distilled water and then scanned in potential between 0.4 and 1.2 V, with a scan rate of 50 mV s^{-1} in blank 10 mL of 0.1 M BRB (pH 5.0) for several cycles until stable voltammetric profiles were achieved. After this process, a solution of known concentration of BPA and BPS (or binary mixture) is added to the electrochemical cell. Eventually, the corresponding data were obtained by CV and SWV techniques. All voltammetric data were collected through three parallel measurements.

Results and Discussion

Characterization of the TETA-Grafted MWCNTs

The FTIR spectrum of MWCNTs and TETA-modified MWCNTs (TETA-MWCNTs) is illustrated in Fig. 1A. The FTIR spectrum profile of MWCNTs (Fig. 1A, curve a) is different from that of TETA-MWCNTs (Fig. 1A curve b). In this case, when MWCNTs were functionalized by TETA, several new adsorption peaks were monitored in the spectrum recognized as follows: the distinctive adsorption bands at 3321 cm^{-1} (–OH stretching oscillation of –COOH), 2957 cm^{-1} ($–CH_2$ stretching oscillation), 1725 cm^{-1} (C = O stretching oscillation), 1637 cm^{-1}, (–NH bending oscillation of –NH– groups on TETA), 1460–1383 cm^{-1} (C–N stretching oscillations) and 1241–1066 cm^{-1} (C–O stretching oscillations), respectively (AlOthman et al. 2015; Vatanpour and Haghighat 2019).

SEM was used to investigate the surface morphology of MWCNTs and TETA-MWCNTs. The SEM images are illustrated in Fig. 1B and C. The surface morphology of the MWCNTs and TETA-grafted MWCNTs exhibits considerable differences. The formation of a porous surface for TETA-grafted MWCNTs is seen (Fig. 1C). The homogenous and porous morphology of TETA-MWCNTs can improve the surface contact area with the target analytes while also facilitating a fast electronic transfer for the electrochemical reactions. By the surface alteration of MWCNTs with TETA in the recommended work, the surface of TETA-grafted MWCNTs has rich in the $–NH_2$ group which ensures nucleophilic features to MWCNTs that activate the surface of MWCNTs for a variety of implementations (Hayat et al. 2022). Consequently, the TETA-MWCNTs architectures were employed to be an optimistic electrode material for the sensing of BPA and BPS as compared to unmodified MWCNTs.

Electrochemical Behavior of BPA and BPS

A binary solution is prepared by mixing BPA (0.1 mM) and BPS (0.1 mM). The voltammetric response of the modified electrodes has been evaluated by the CV technique. Figure 2 A showed the CVs of EDCs on (a) naked GCE, (b) ox-MWCNTs/GCE, and (c) TETA-MWCNTs/GCE, respectively. As illustrated in Fig. 2A, the electrochemical response of EDCs on naked GCE was smaller (curve a), and two oxidation peaks of BPA and BPS located at 0.748 V and 1.040 V were observed, and the peak currents were 1.66 µA and 0.75 µA, respectively, and the electro-oxidation processes were irreversible characters. The oxidation current

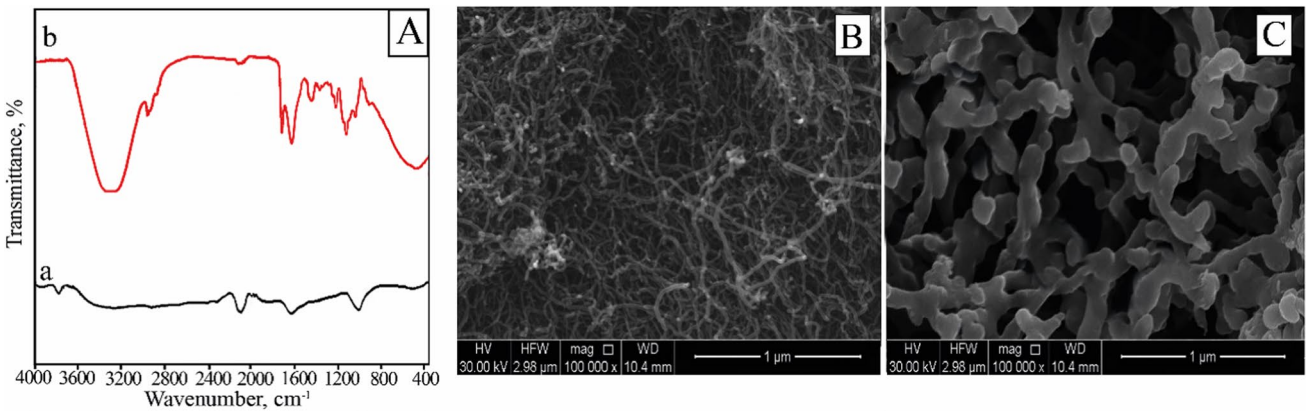

Fig. 1 **A** FTIR spectra of MWCNTs (a), TETA-MWCNTs (b). **B** SEM images of ox-MWCNTs. **C** TETA-MWCNTs

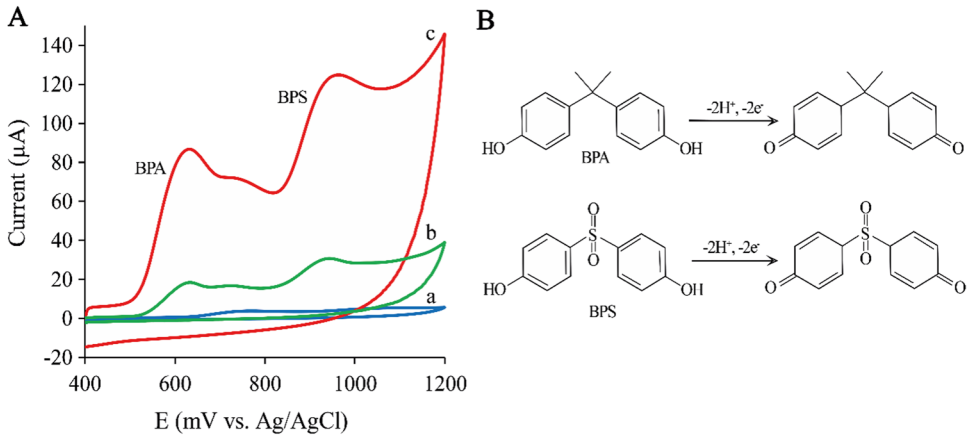

Fig. 2 **A** CVs for BPA (0.1 mM) and BPS (0.1 mM) binary solutions recorded at bare GCE (a), ox-MWCNTs/GCE (b), and TETA-MWCNTs/GCE (c) in 0.1 M BRB (pH 5) at a scan rate 50 mV/s. **B** Proposed electrode process schemes of BPA and BPS at the TETA-MWCNTs/GCE

responses for EDC at ox-MWCNTs/GCE (b) are 13 and 11 μA; however, at TETA-MWCNTs/GCE (c), they are 56 and 35 μA, respectively. Compared with the naked GCE, these three modified GCEs exhibited electrocatalytic activity for the oxidation of EDCs. Moreover, a negative potential shift has been monitored for both analytes on (b) ox-MWCNTs/GCE, (c) TETA-MWCNTs/GCE as follows; BPA: 632 to 612 mV and BPS: 943 to 931 mV. It should be demonstrated that the electrochemical activity of TETA-MWCNTs was better than that of MWCNT-COOH due to the better dispersion behavior of TETA-MWCNT architecture. The possible mechanism for the electrochemical oxidation of each analyte is presented in Fig. 2B.

Effect of Scan Rate

Helpful knowledge involving the voltammetric reaction mechanism can be mostly achieved from the relationship between peak intensity (I_p) and a scan rate of potential (ν) in CV. Thereby, the influence of potential scan rates (v) on the anodic currents (I_p) of 0.1 mM BPA and 0.1 mM BPS at the TETA-grafted MWCNTs/GCE in 0.1 M BRB was individually examined by CV (Fig. 3). In this context, the CV experiments at dissimilar scan rates from 10 to 200 mV/s were studied. The plot of anodic peak current versus the scan rate was linear when the scan rate increased from 25 to 200 mV/s, which proves that the electrochemical oxidation of two analytes on the TETA-grafted MWCNTs/GCE sensor is an adsorption-controlled process. The regression equation was found as: I_{BPA} (μA) = 0.902 v (mV/s) + 14.244 (R^2 = 0.9965) for BPA and I_{BPS} (μA) = 0.5909 v (mV/s) + 39.902 (R^2 = 0.9962) for BPS. The dependence of E_{pa} with ln$v$ can be expressed as E_{pa} (V) = 0.0251 ln$v$ (mV/s) + 0.573 (R^2 = 0.9912) for BPA and E_{pa} (V) = 0.0253 ln$v$ (mV/s) + 0.864 (R^2 = 0.9926) for BPS. In addition, in the scan rate range from 25 to 200 mVs^{-1}, peak currents (I_p) of BPA and BPS electrooxidation depend linearly on square root of the scan rate ($v^{1/2}$) and are described by the equation: I_{BPA} (μA) = 18.581 $v^{1/2}$ (mV/s) − 30.31 (R^2 = 0.9945) and I_{BPS} (μA) = 11.362 $v^{1/2}$ (mV/s) − 8.1757 (R^2 = 0.9938). This fact can suggest that the electrode process of BPA and BPS electrooxidation is not controlled by diffusion and can be preceded by a chemical reaction. On the other

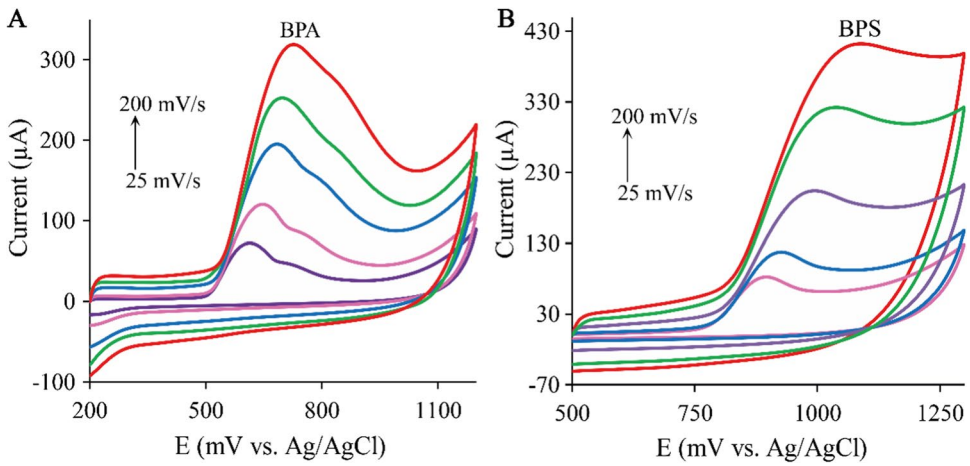

Fig. 3 CVs of 0.1 mM BPA (**A**) and 0.1 mM BPS (**B**) in 0.1 M BRB (pH 5) at different scan rates from 25 to 200 mV/s (25, 50, 100, 150, and 200 mV/s) at TETA-MWCNTs/GCE

hand, a dependence of ln I_p on ln v is linear and described by the equations: ln I(μA) = 0.6011 ln v (mV/s) + 0.9624 (R^2 = 0.9977) for BPA and ln I(μA) = 0.6302 ln v (mV/s) + 0.96 (R^2 = 0.9963) for BPS. Its slope is 0.6 and indicates adsorption-control of the electrode process. A slope close to 0.5 is expected for diffusion-controlled electrode processes and close to 1.0 for adsorption-controlled processes (Bard and Faulkner 2001; Brett and Brett 1993). This linearity demonstrated that the redox reaction of BPA and BPS was a typical adsorption-controlled process. The obtained results confirm the above findings. As exhibited by growing the scan rate, the anodic peak potential value of both analytes shifted to a more positive value of potential. For a fully irreversible and adsorption-controlled process, Laviron's equation (Eq. 1) can be employed to calculate α and n. According to the equation (E_p versus ln v) (Eq. 1), the value of RT/αnF was found to be 0.0251 for BPA and 0.0251 for BPS. Since for a fully irreversible electron transfer, α was assumed as 0.5. Based on Eq. (1), the transfer electron number was 2.05 for BPA and 2.03 for BPS in the rate-determination step, respectively.

$$E_p = A + RT/(1-\alpha)nFlnv \quad (1)$$

In this equation, F = Faraday's constant (96,485.339 C/mol), R = universal gas constant (8.31447 J K^{-1} mol^{-1}), T = absolute temperature, α = electron transfer coefficient, n = electron transfer numbers, ln$v$ = scan rate in mV/s, A = the constant value.

Electrochemical Impedance Spectroscopy Characterization of the Sensor

Electrochemical impedance spectroscopy was applied to display the achievement of the electrochemical sensor prepared at each stage of the electrode modification process. Figure 4 A displays the typical EIS (Nyquist diagrams) results at the surface of (green curve) GCE, (red curve) ox-MWCNTs/GCE, (blue curve) TETA-MWCNTs/GCE in a mixture of 5.0 mM $[Fe(CN)_6]^{3-/4-}$ and 0.1 M KCl. The frequency bands were between 0.1 Hz and 0.1 MHz. The electron-transfer resistance (R_{et}) of naked GCE was calculated to be 706 Ω (green curve). The R_{et} value of naked GCE was more than (red curve) ox-MWCNTs/GCE and (blue curve) TETA-MWCNTs/GCE. On the other hand, the R_{et} value of the ox-MWCNTs/GCE was estimated to be 21.8 Ω (blue curve). The semicircle part, as observed at higher frequencies, was associated with a process that was limited by electron transfer. The linear features observed at lower frequencies were attributed to diffusion-limited electron transfer. The covalent binding of TETA on the ox-MWCNTs to fabricate TETA-MWCNTs/GCE caused a remarkable decrease of the semicircle portion at higher frequencies to form a nearly-straight line (Fig. 4A, blue curve). This may be demonstrated that the TETA-MWCNTs layer introduced an advantage to the interfacial electron transfer. Because of the positive charge of TETA in the layer, the $[Fe(CN)_6]^{4-/3-}$ probe could arrive at the surface of the electrode promptly. The impedance changes of the different modified electrodes revealed that TETA had

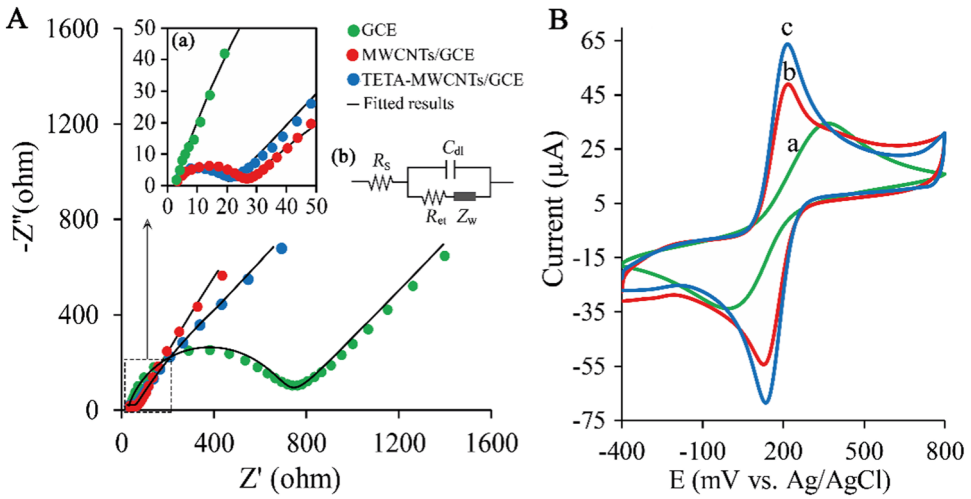

Fig. 4 **A** Nyquist plot of experimental (colored symbols) and fitted results (black lines). EIS curves of the three electrodes (bare GCE (green curve), ox-MWCNTs/GCE (red curve), and TETA-MWCNTs/GCE (blue curve) measured in 0.1 mol/L KCl containing 5.0 mM $Fe(CN)_6^{3-/4-}$ over the frequency range of 0.1 MHz to 0.1 Hz with an amplitude of 5 mV. The insert in (a) shows the quasi-vertical curve in the low-frequency region. The insert in (b) shows an equivalent circuit model applied to fit the Nyquist plots quantitatively. R_{ct}, charge transfer resistance; R_S, electrolyte solution resistance; Z_W, Warburg impedance resulting from the diffusion of ions; C_{dl}, double-layer capacitance of the electrode. **B** CV curves of the three electrodes in 0.1 mol/L KCl containing 3.0 mM $Fe(CN)_6^{3-/4-}$, scan rate 50 mV/s

attached to the ox-MWCNTs. EIS result indicated that a GCE modified with the TETA-MWCNTs nanocomposite displayed an excellent electrochemical performance than the naked GCE and ox-MWCNTs-modified GCE. The findings display that the TETA-MWCNTs/GCE exhibits faster electron-transfer kinetics and a large number of redox sites compared to other modified electrodes. The TETA is known to form a stable nitrogen source to make nitrogen-rich MWCNTs (Narwade et al. 2021). The findings show that the TETA-MWCNTs have higher electrochemical performance than ox-MWCNTs/GCE. It enhances the voltammetric efficiency due to improving charge transfer and high electrochemical activity. The results suggest that BPA and BPS can be efficiently detected by the TETA-MWCNTs-modified GCE.

CV Characterization of the Sensor

The CV behavior of different modified electrodes in a mixture of 3.0 mM $K_3[Fe(CN)_6]$ and 3.0 mM $K_4[Fe(CN)_6]$ solution is displayed in Fig. 4B. A single pair of the reversible peak of ferricyanide ions can be monitored on the naked GCE (curve a) and the ΔEp ($\Delta Ep = E_{pa}\text{-}E_{pc}$) value obtained was 375 mV. Manifestly increased reversible peak current was monitored on the ox-MWCNTs-modified GCE (curve b) and the ΔEp value of the redox probe was decreased to 92 mV. When the naked GCE was carefully altered with TETA-grafted MWCNTs (curve c), the redox peak current increased markedly, and the monitored ΔEp value was decreased to 80 mV. With the TETA-MWCNTs/GCE, the CV profile (versus $Fe(CN)_6^{3-/4-}$probe) displays a higher current response than ox-MWCNTs/GCE. These results show that TETA-MWCNTs have a higher proportion of electroactive or redox sites than ox-MWCNTs and bare electrodes. The TETA-MWCNTs electrode has the lowest R_{ct} and lowest ΔE_p, while ox-MWCNTs have a higher R_{ct} and higher ΔE_p. Thus, the TETA-MWCNTs surface has better electrochemical reactivity. Based on the above findings, we can approve that our fabrication duration was feasible.

Furthermore, the Randles–Sevcik equation (Eq. 2) was also employed to estimate the specific surface area of TETA-MWCNTs/GCE from the CV result of the $Fe(CN)_6^{3-/4-}$ redox probe.

$$I_p = \left(2.69 \times 10^5\right) n^{3/2} D_0^{1/2} C_0 v^{1/2} A \tag{2}$$

In this equation, I_p = peak current (amperes), n = number of electrons transferred in a redox cycle, A = the electroactive surface area (cm^2), C_0 = molar concentration of redox-active species (mol/cm^3), D_0 = the diffusion coefficient (6.6×10^{-6} cm^2/s) (Wang 2006), v = scan rate in V/s. Based on Eq. (2), the calculated electroactive surface area was 0.0629 cm^2 and 0.6000 cm^2 for naked GCE and TETA-MWCNTs/GCE, respectively. The noticeable growth of the electroactive surface area of TETA-MWCNTs/GCE, attended by facilitated electron transfer, enables to increase in the efficiency of the occurring electrode reaction, and so that manifests in an outstanding increase of peak current and thus higher sensitivity.

Importantly, the use of the Randles–Sevcik equation is not the most appropriate method for electroactive area estimation because ($i_{p)}$ is proportional to the scan rate. If the scan rate changes, probably i_p will be changed too. The electroactive area is a physical parameter and it does not change with scan rate. Therefore, the thickness of the diffusion layer can be calculated from Eq. (3) (Bard and Faulkner 2001).

$$\delta = \sqrt{\pi D t} \tag{3}$$

where the δ is the thickness of the diffusion layer reported in cm, D is the diffusion coefficient of the redox probe (cm^2 s^{-1}), and t is the timescale experiment for the forward scan (s). The parameters used in the experiments are as follows: $D = 6 \times 10^{-6}$ cm s^{-1} (Smith et al. 2015) and $t = 15$ s. The thickness of the diffusion layer value calculated from Eq. (3) for these experimental conditions was 168 µM. This calculated thickness is much larger than the scale of nanomaterial surface roughness.

Effect of pH

Initially, the effect of supporting electrolyte type was investigated. In this context, various buffer solution was tested such as phosphate buffer (PBS) (a), acetate buffer (ACB) (b), and BRB (c) (each 0.1 M, pH 5). According to the test results, the maximum current response was observed in BRB as shown in Fig. 5(A and B). Therefore, BRB was chosen as a supporting electrolyte. The influence of pH on the peak current of BPA (Fig. 5C) and BPS (Fig. 5D) at TETA-MWCNTs/GCE was properly studied with the pH value of supporting electrolytes ranging from 3.0 to 7.0. As illustrated in Fig. 5E, the oxidation peaks of BPS increased apparently from pH 3.0 to pH 5.0. However, up to the increase of solution pH, the oxidation peak current of BPA increased slightly till pH = 5. In this case, at pH 5 ($I_p \sim 80$ µA), the response of BPA is slightly higher than at pH 3 ($I_p \sim 76$ µA). As can be seen in Fig. 5E, the peak currents in pH = 5.0 are maximum; therefore, pH = 5.0 was selected as the optimum pH, and this pH was used in all following experiments. While the pH value was over 6.0, the peak currents of the two analytes were decreased. The regression equation (E(V) versus pH) was estimated to be as follows: $E(V) = -0.0637$ pH + 0.9502 ($R^2 = 0.9979$) for BPA and $E(V) = -0.0665$ pH + 1.2433 ($R^2 = 0.9904$) for BPS. Based on the above equations, the measured value (63.7 and − 66.5 V/pH) is close to the theoretical or known value of 59.0 mV/pH,

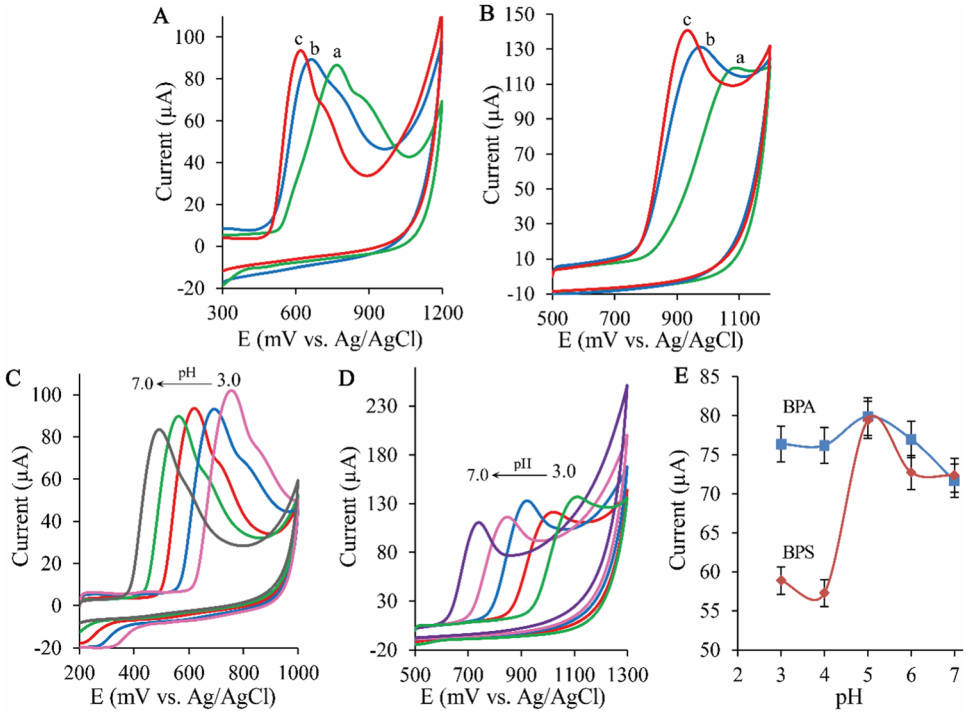

Fig. 5 CV for 0.1 mM BPA (**A**) and 0.1 mM BPS (**B**) in different supporting electrolyte (0.1 M) PBS (a), ACB (b), and BRB (c) at a scan rate 50 mV/s. CVs of 0.1 mM BPA (**C**) and BPS (**D**) in 0.1 M BRB with different pH values (3.0–7.0) on the TETA-MWCNTs/GCE at a scan rate of 50 mV/s. **E** Linear relation between the peak potentials (E_{pa}) and the pH values. Error bars represent standard deviations ($n = 3$)

indicating the involvement of an equal number of electrons and protons. The pH with optimum response was lower than the pKa of BPA (pKa = 9.6–10.2 (Li et al. 2016b)) and BPS (pKa = 8.20) (Guo et al. 2016), informing that the undissociated analyte (BPA and BPS) can be more easily adsorbed than thedissociated EDCs on the modified GCE surface.

BPA molecule exists in different molecular structures with different charge distributions, depending on the pH of the solution. At low and neutral pH, BPA exists predominantly in its neutral form HO–$C_{15}H_{14}$–OH, while above pH 10.1, the negatively charged species HO–$C_{15}H_{14}$–O − (phenolate) predominates. On the other hand, although, phenolate remains the single dominant species in water at pH > 10.1. In this system, at pH (3.0–7.0), BPA has a main peak at 612 mV with a secondary peak (725 mV) or shoulder about 113 mV higher. The two peaks may correspond to the oxidation of two species (neutral BPA and phenolate) (Del Olmo et al. 1998; Kuramitz et al. 2001; Schäfer et al. 2006). Although, the minor peak slightly increases and then decreases (pH > 7) with the increasing pH value of the BRB. This result shows that the phenolate ion is oxidized more easily than neutral BPA. These results are in good agreement with a previously reported method (Wang et al. 2018). Consequently, for the simultaneous and sensitive sensing of BPA and BPS, 0.1 M BRB with a pH of 5.0 was chosen as the supporting electrolyte. The above findings demonstrated that the modified GCE had a high electrochemical performance for the oxidation of BPA and BPS in 0.10 M BRB (pH 5.0).

Simultaneous Detection of BPA and BPS

Before recording the linear curve for BPA and BPS detection, the frequency (1–10 Hz), step size (5–20 mV), and pulse amplitude (50–200 mV) were carefully examined in the detection of both compounds. The optimal parameter values were frequency: 4 Hz, step size: 15 mV, and pulse amplitude: 150 mV.

Binary solutions have been prepared from various concentrations of both analytes in the range 1.0 − 30 μM using 0.1 M BRB, and SWV was employed for the simultaneous detection of BPA and BPS. The detection of two analytes was carried out by the simultaneous increase of their concentrations. It can be monitored in Fig. 6 that the responses of two analytes increased when the concentrations simultaneously increased within the linear range of 1.0 − 30 μM. The findings indicated that the developed sensor can be properly used for the simultaneous sensing of two EDCs without interference with each other. In Fig. 6A, the linear correlation between their SWV responses and concentration can be described as follows: I(μA) = 1.9543 C (μM) + 1.8539 ($R^2 = 0.9974$) for BPA and I(μA) = 1.0709 C (μM) + 3.7099 ($R^2 = 0.9925$) for BPS. Additionally, the LODs of BPA and BPS were 0.35 μM and 0.56 μM, respectively. The LOD was calculated based on LOD = 3SD/m (Miller and Miller 1993). In this equation, SD is the standard deviation of a concentration of 1.0 μM (binary solution, each 1.0 μM) measured with five replicates and *m* is the slope of the calibration plot. Electrochemical findings exhibit that the TETA-MWCNTs textures with a perfectly active surface area is a promising

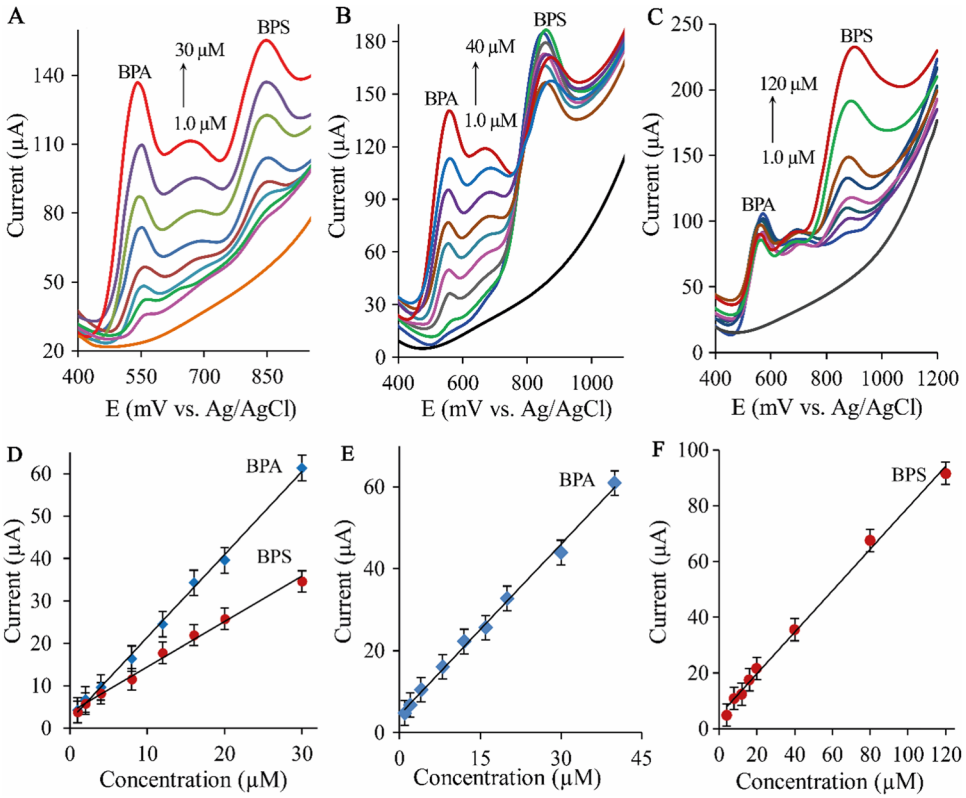

Fig. 6 **A** SWV for various BPA and BPS concentrations in a binary mixture in the range 1.0–30 µM in 0.1 M BRB at TETA-MWCNTs/GCE. **B** SWV on the TETA-MWCNTs/GCE in 0.1 M BRB (pH 5.0) containing 20 µM BPS and different concentrations of BPA (0.0, 1.0, 2.0, 4.0, 8.0, 12, 16, 20, 30, and 40 µM). **C** SWV on the TETA-MWCNTs/GCE in 0.1 M BRB (pH 5.0) containing 20 µM BPA and different concentrations of BPS (0.0, 1.0, 4.0, 8.0, 16, 20, 40, 80, 120 µM). **D** Calibration plot of peak current versus BPA and BPS concentrations for simultaneous detection. **E** Calibration plot of peak current versus BPA concentrations for individual detection. **F** Calibration plot of peak current versus BPS concentrations for individual detection. SWV parameters: frequency 4 Hz, step size 15 mV, pulse size 150 mV. Error bars represent standard deviations ($n = 3$)

scaffold for the detection of a binary mixture of BPA and BPS with limits of detection in the µM range (0.35 µM and 0.56 µM, respectively). These µM LODs are interrelated to the sensitivity and differentiation behavior of the synthesized TETA-MWCNTs/GCE for these coexisting practiced two analytes even at small concentrations.

Individual sensing of both analytes was shown in Fig. 6(B and C). Thereby, the quantitative assessment of BPA and BPS at the TETA-MWCNTs/GCE, SWV was performed with a contrariwise binary mixture in BRB pH 5 under optimized experimental conditions. To measure the current response of one analyte, the other target analyte was fixed in a specific concentration. For individual sensing BPA, BPA concentration was increased gradually from 1.0 to 40 µM, in the presence of BPS (BPS was fixed at 20 µM). The responses of BPA increased linearly with the increasing concentrations, while the BPS peak current was nearly stable. In the range from 1.0 to 40 µM, BPA concentration reveals a good linear relationship with the oxidation peak currents. Figure 6B shows the increase in the peak currents of BPA. Similarly, for sensing BPS, BPS concentration was changed gradually from 1.0 to 120 µM, in the presence of BPA (BPA was fixed at 20 µM). As a result, BPS concentration with the range from 1.0 to 120 µM and the current value also display a good linear relationship. Figure 6C shows the increase in the peak currents of BPS. These reached results allow concluding that the change of concentration of one analyte did not have an important effect on the SWV response of the other one, showing that their peak currents are independent. As a function of concentration (from Fig. 6B and C), the linear equation was: I_{pa} (µA) = 1.3893 C (µM) + 4.3109 ($R^2 = 0.9964$) for BPA and I_{pa} (µA) = 0.7445 C (µM) + 4.8107 ($R^2 = 0.9953$) for BPS. The LODs were calculated as 0.26 µM for BPA and 0.72 µM for BPS based on the LOD = 3SD/m.

Comparison of the Proposed Method

The analytical characteristics of different voltammetric sensors for the simultaneous sensing of two EDC compounds are exhibited in Table 1. Compared to early published sensors for the simultaneous detection and quantification of two EDCs, our developed voltammetric sensor has a lower LOD (the calculated LOD for BPA and BPS are 0.35 µM and 0.56 µM, respectively). The LOD values are lower than those previously reported in the kinds of literature (Zheng et al. 2016; Wang et al. 2018). Also, the TETA-MWCNTs-modified GCE displays a wide linear range than previously used methods (Zheng et al. 2016; Wang et al. 2018). However, it should be pointed out that the fabrication of modified electrodes is often time-consuming involves various complicated steps (except Wang et al. 2018) and sometimes leads to nonreproducible results (Zheng et al. 2016; Ye et al. 2019; Pang et al. 2020). In our experiments, usage

Table 1 Examples from the previously reported strategies for simultaneous electrochemical determination of BPA and BPS

Sensor	Linear range (μM)		LOD (μM)		Reference
	BPA	BPS	BPA	BPS	
Pt/PDDA-DMP hybrid/GCE	5–30	10–60	0.6	2.0	Zheng et al. (2016)
MWCNTs/GCE	2–30	20–80	0.5	4.0	Wang et al. (2018)
CTpPa-2/GCE	0.1–50	0.5–50	0.02	0.09	Pang et al. (2020)
AuAgPt-PCD-GO/GCE	0.006–4.0	0.008–8	0.002	0.00267	Ye et al. (2019)
TETA-MWCNTs/GCE	1.0–30	1.0–30	0.35	0.56	This work

AuAgPt, AuAgPt ternary alloy nanocrystals; *CTpPa-2*, covalent organic framework (Tp:1,3,5-triformylphloroglucinol; *CTp*, chiral (þ)-diacetyl-L-tartaric anhydride; *Pa-2*, 2,5-dimethyl-p-phenylenediamine); *DMP*, diamond powder; *GCE*, glassy carbon electrode, *GO*, graphene oxide, *MWCNTs*, multi-walled carbon nanotubes; *PCD*, porous β-cyclodextrin polymer; PDDA, poly(diallyl dimethyl ammonium chloride); *Pt*, platinum nanoparticles

of TETA-MWCNTs-modified GCE decreases the risk of measurement errors (a small number of operations in the analytical procedure) and reduces the expenses and operational skills of analysts.

Reproducibility, Repeatability, and Stability

Five independent TETA-MWCNTs/GCEs were used to measure the reproducibility of electrodes. The results showed that five independent TETA-MWCNTs/GCEs had very similar detection results for BPA and BPS (each 8 μM). The relative standard deviation (RSD) was found to be 4.2% for BPA and 5.2% for BPS. In addition, the oxidation peak current response of the prepared electrode for BPA and BPS (each 8 μM) was retained at about 94% and 93% of its initial current after 4 weeks storage (in a refrigerator at 4 °C). As noticed in the CV, the electrochemical oxidation of BPA and BPS is an irreversible process, and its oxidation products are likely to adsorb on the electrode surface, thereby reducing the electrochemically active area. Therefore, the TETA-MWCNTs/GCE is not a repeatable electrochemical sensor. The above findings indicated that the TETA-MWCNTs-modified GCE has excellent coincidence so using it to estimate the concentration of EDCs simultaneously will have good reproducibility and accuracy. Based on the well electrochemical property, the TETA-MWCNTs nanocomposites can be used as a new class of electrode material for electrochemical applications, so the tests of reproducibility and stability are very important.

Interference Studies

One crucial issue for the practicality of a sensor is its proficiency to differentiate the target species from foreign species. Therefore, the voltammetric responses of BPA and BPS (8 μM each) were carefully measured at the TETA-MWCNTs/GCE in the presence of different foreign species. The reached findings indicate that the prevalent inorganic species such as Ca^{2+}, Mg^{2+}, Zn^{2+}, Al^{3+}, Cu^{2+}, K^{+}, Na^{+}, Cl^{-} and SO_4^{2-} in 100-fold excess almost do not affect the current response of both analytes at the TETA-MWCNTs/GCE (Fig. 7A). Furthermore, the effects of some potential organic species (tenfold excess) such as glucose, uric acid, and ascorbic acid on the SWV response of both molecules were properly tested. The experimental findings indicate that these two analytes do not give rise to a definable change in peak currents of BPA and BPS. To further verify the selectivity of the TETA-MWCNTs/GCE to BPA and BPS, imipramine, desipramine (antidepressant drugs), organophosphate, organochloride (pesticides), and estradiol were selected as the interferents. According to the experimental results, no significant interferences were also observed in the tenfold excess of commonly available molecules such as imipramine, desipramine, organophosphates, organochlorides, and estradiol (Fig. 7B). Consequently, the introduced TETA-MWCNT-based voltammetric sensor has sufficient selectivity and satisfactory anti-interference performance for the accurate sensing of target EDCs.

Real Food Samples Analysis

To understand the potential implementation, the designed sensor was applied to estimate BPA and BPS in drinking water, milk, cola, and juice samples. Accuracy studies were tested by determining the recovery of spiked two analytes to the matrix of the samples. The specific concentrations of standard two analytes were appropriately spiked into the abovementioned samples, and three replicate experiments were performed to display the recovery efficiency. The obtained findings were illustrated in Table 2. It can be displayed that the recovery values of BPA and BPS were from 94 to 98%. The experimental findings demonstrated that TETA-MWCNT/GCE could serve as a voltammetric sensor for simultaneous detection of BPA and BPS in real food samples.

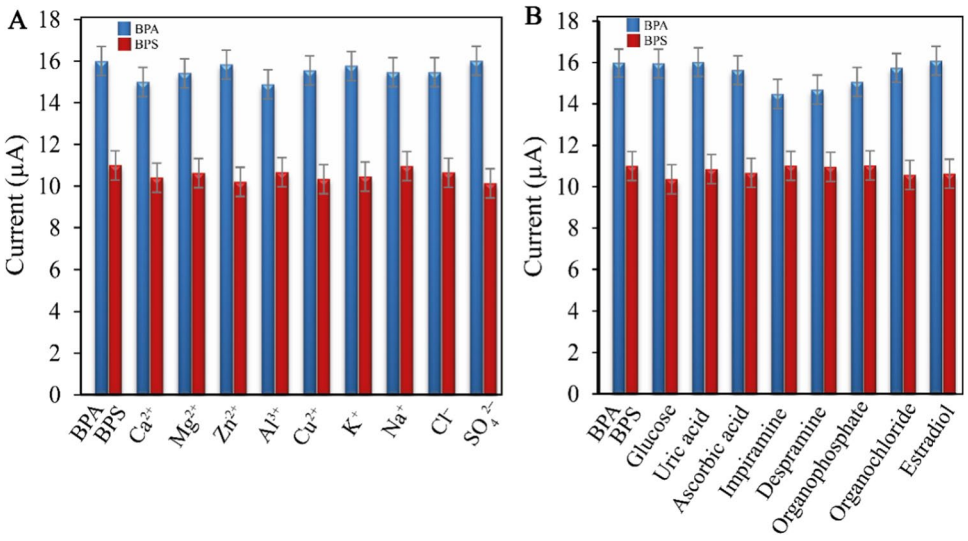

Fig. 7 Comparison of the current response of TETA-MWCNTs/GCE with 8 μM BPA and BPS in the absence or presence of selected foreign species. **A** 100-fold. **B** tenfold. Error bars represent standard deviations ($n=3$)

Table 2 Simultaneous detection of BPA and BPS in food samples using TETA-MWCNTs/GCE ($n=3$)

Sample	Added (μM)	Found (μM) ± SD		Recovery (%)	
		BPA	BPS	BPA	BPS
Water	-	< LOD	< LOD	-	-
	8	7.86 ± 0.35	7.83 ± 0.21	98.25	97.88
	12	11.95 ± 0.63	11.82 ± 0.25	99.58	98.50
	20	20.05 ± 0.48	19.61 ± 0.42	100.25	98.05
Milk	-	< LOD	< LOD	-	-
	8	7.57 ± 0.45	7.65 ± 0.45	94.63	95.63
	12	11.64 ± 0.22	11.64 ± 0.40	97.00	97.00
	20	19.86 ± 0.13	19.53 ± 0.32	99.30	97.65
Cola	-	< LOD	< LOD	-	-
	8	7.86 ± 0.32	7.72 ± 0.36	98.25	96.50
	12	11.72 ± 0.36	11.81 ± 0.24	97.67	98.42
	20	19.84 ± 0.17	19.58 ± 0.45	99.20	97.90
Juice	-	< LOD	< LOD	-	-
	8	7.56 ± 0.26	7.65 ± 0.36	94.50	95.63
	12	11.95 ± 0.23	11.54 ± 0.51	99.58	96.17
	20	20.05 ± 0.12	18.88 ± 0.72	100.25	94.40

Conclusion

In this current protocol, we have introduced the electrochemical behavior of BPA and BPS at TETA-MWCNTs/GCE. MWCNT increased the surface area as well as formed TETA-MWCNT adsorption sites for BPA-BPS, which improved sensor sensitivity. The developed sensor shows outstanding electrochemical efficiency for simultaneous sensing and quantification of both analytes with a large anodic peak potential difference. Moreover, the proposed method has been successfully applied for the detection of BPA and BPS in a variety of food samples with satisfactory results. Furthermore, the fabrication of TETA-MWCNTs not only encourages the development of new porous textures but also ensures a new vision for the design of electrochemical-based sensors. The sensor was able to detect BPA-BPS in the presence of different interfering nontarget species (e.g., Cl^-, Mg^{2+} Ca^{2+}, and various organic compounds), and was also able to detect BPA-BPS in a pH-adjusted food matrix with convincing sensitivity. The invented method will be useful for the detection of BPA and BPS in food products and thus would be of great help to food quality control and monitoring. Finally, the invented electrochemical sensor can be used for monitoring water pollution control.

Acknowledgements The authors gratefully acknowledge the use of the facilities of Istanbul University-Cerrahpaşa (Istanbul/Turkey).

Author Contribution Maşide Çakıcı: performed the measurements, processed the experimental data, performed the analysis, and designed the figures. Asiye Aslıhan Avan: performed the measurements, processed the experimental data, performed the analysis, and designed the figures. Hayati Filik: drafted the manuscript and involved in planning and supervised the work, aided in interpreting the results, and worked on the manuscript. Ece Kök Yetimoğlu: processed the experimental data. All authors discussed the results and commented on the manuscript.

Data Availability The dataset analyzed during the current study is available from the corresponding author on reasonable request.

Declarations

Competing Interests The authors declare no competing interests.

Ethics Approval This article does not contain any studies with human participants or animals performed by any of the authors.

Conflict of Interest Maşide Çakıcı declares that he has no conflict of interest. Asiye Aslıhan Avan declares that he has no conflict of interest. Hayati Filik declares that he has no conflict of interest. Ece Kök Yetimoğlu declares that he has no conflict of interest.

Informed Consent Informed consent is not applicable.

References

AlOthman ZA, Yilmaz E, Habila MA, Alsohaimi IH, Aldawsari AM, Al-Harbi NM, Soylak M (2015) Triethylenetetramine modified multiwalled carbon nanotubes for the efficient preconcentration of Pb(II), Cu(II), Ni(II) and Cd(II) before FAAS detection. RSC Adv 5:106905–106911. https://doi.org/10.1039/C5RA19213G

Avan AA, Filik H (2018) $CoFe_2O_4$-MWCNTs modified screen printed carbon electrode coupled with magnetic $CoFe_2O_4$-MWCNTs based solid phase microextraction for the detection of bisphenol A. Curr Nanosci 14:199–208. https://doi.org/10.2174/1573413713666171109160816

Baccarin M, Ciciliati MA, Oliveira ON, Cavalheiro ETG, Raymundo-Pereira PA (2020) Pen sensor made with silver nanoparticles decorating graphite-polyurethane electrodes to detect bisphenol-A in tap and river water samples. Mater Sci Eng C 114:110989. https://doi.org/10.1016/J.MSEC.2020.110989

Baluka SA, Rumbeiha WK (2016) Bisphenol A and food safety: lessons from developed to developing countries. Food Chem Toxicol 92:58–63. https://doi.org/10.1016/J.FCT.2016.03.025

Bard AJ, Faulkner LR (2001) Electrochemical methods: fundamentals and applications, 2nd edn. John Wiley & Sons

Brett CMA, Brett AMO (1993) Electrochemistry — principles, methods and applications. Oxford University Press, Oxford

Butmee P, Tumcharern G, Saejueng P, Stankovic D, Ortner A, Jitcharoen J, Kalcher K, Samphao A (2019) A direct and sensitive electrochemical sensing platform based on ionic liquid functionalized graphene nanoplatelets for the detection of bisphenol A. J Electroanal Chem 833:370–379. https://doi.org/10.1016/J.JELECHEM.2018.12.014

Campos AM, Raymundo-Pereira PA, Cincotto FH, Canevari TC, Machado SAS (2016) Sensitive determination of the endocrine disruptor bisphenol A at ultrathin film based on nanostructured hybrid material SiO_2/GO/AgNP. J Solid State Electrochem 20:2503–2507. https://doi.org/10.1007/S10008-015-3098-Y

Canevari TC, Rossi MV, Alexiou ADP (2019) Development of an electrochemical sensor of endocrine disruptor bisphenol A by reduced graphene oxide for incorporation of spherical carbon nanoparticles. J Electroanal Chem 832:24–30. https://doi.org/10.1016/J.JELECHEM.2018.10.044

de Sá AC, Barbosa SC, Raymundo-Pereira PA, Wilson D, Shimizu FM, Raposo M, Oliveira ON Jr (2020) Flexible carbon electrodes for electrochemical detection of bisphenol-A, hydroquinone and catechol in water samples. Chemosens 8:103. https://doi.org/10.3390/CHEMOSENSORS8040103

Del Olmo M, Zafra A, Gonzalez-Casado A, Vilchez JL (1998) The use of β-cyclodextrin inclusion complexes for the analysis of bisphenol a residues in water by Spectrofluorimetry. Int J Environ Anal Chem 69:99–110. https://doi.org/10.1080/03067319808032577

Dubey R, Dutta D, Sarkar A, Chattopadhyay P (2021) Functionalized carbon nanotubes: synthesis, properties and applications in water purification, drug delivery, and material and biomedical sciences. Nanoscale Adv 3:5722–5744. https://doi.org/10.1039/D1NA00293G

Ezoji H, Rahimnejad M (2018) Electrochemical behavior of the endocrine disruptor bisphenol A and in situ investigation of its interaction with DNA. Sens Actuators B Chem 274:370–380. https://doi.org/10.1016/J.SNB.2018.07.147

Filik H, Avan AA, Yetimoğlu EK (2019) Multiwalled carbon nanotubes β-cyclodextrin modified electrode for electrochemical determination of bisphenol S in water samples. Russ J Electrochem 55:70–77. https://doi.org/10.1134/S1023193519010038

Filik H, Avan AA (2017) Electrochemical determination of bisphenol a based on poly(Chromotropic acid) modified glassy carbon electrode. Curr Anal Chem 13https://doi.org/10.2174/1573411013666161214112952

García-Córcoles MT, Cipa M, Rodríguez-Gómez R, Rivas A, Olea-Serrano F, Vílchez JL, Zafra-Gómez A (2018) Determination of bisphenols with estrogenic activity in plastic packaged baby food samples using solid-liquid extraction and clean-up with dispersive sorbents followed by gas chromatography tandem mass spectrometry analysis. Talanta 178:441–448. https://doi.org/10.1016/J.TALANTA.2017.09.067

González EA, Gulppi M, Páez MA, Zagal JH (2016) O_2 reduction on electrodes modified with nitrogen doped carbon nanotubes synthesized with different metal catalysts. Diam Relat Mater 64:119–129. https://doi.org/10.1016/J.DIAMOND.2016.02.003

Guo H, Li H, Liang N, Chen F, Liao S, Zhang D, Wu M, Pan B (2016) Structural benefits of bisphenol S and its analogs resulting in their high sorption on carbon nanotubes and graphite. Environ Sci Pollut Res 23:8976–8984. https://doi.org/10.1007/S11356-016-6040-7

Hayat M, Shah A, Nisar J, Shah I, Haleem A, Ashiq MN (2022) A novel electrochemical sensing platform for the sensitive detection and degradation monitoring of methylene blue. Catalysts 12:306. https://doi.org/10.3390/CATAL12030306

Huang R, Liu Z, Yin H, Dang Z, Wu P, Zhu N, Lin Z (2018) Bisphenol A concentrations in human urine, human intakes across six continents, and annual trends of average intakes in adult and child populations worldwide: a thorough literature review. Sci Total Environ 626:971–981. https://doi.org/10.1016/J.SCITOTENV.2018.01.144

Kuramitz H, Nakata Y, Kawasaki M, Tanaka S (2001) Electrochemical oxidation of bisphenol A. Application to the removal of bisphenol A using a carbon fiber electrode. Chemosphere 45:37–43. https://doi.org/10.1016/S0045-6535(01)00032-7

Laviron E (1974) Adsorption, autoinhibition and autocatalysis in polarography and in linear potential sweep voltammetry. J Electroanal Chem Interfacial Electrochem 52:355–393. https://doi.org/10.1016/S0022-0728(74)80448-1

Li T, Cui Z, Yuan W, Li CM (2016a) Ionic liquid functionalized carbon nanotubes: metal-free electrocatalyst for hydrogen evolution reaction. RSC Adv 6:12792–12796. https://doi.org/10.1039/C5RA25460D

Li Y, Zhai X, Liu X, Wang L, Liu H, Wang H (2016b) Electrochemical determination of bisphenol A at ordered mesoporous carbon modified nano-carbon ionic liquid paste electrode. Talanta 148:362–369. https://doi.org/10.1016/J.TALANTA.2015.11.010

Li T, Tang D, Cui Z, Cai B, Li D, Chen Q, Li CM (2018) Functionalized carbon nanotubes for highly active and metal-free electrocatalysts in hydrogen evolution reaction. Electrocatalysis 9:573–581. https://doi.org/10.1007/S12678-017-0452-0

Li Z, Wang L, Li Y, Feng Y, Feng W (2019) Carbon-based functional nanomaterials: preparation, properties and applications. Compos Sci Technol 179:10–40. https://doi.org/10.1016/J.COMPSCITECH.2019.04.028

Lu X, Wang X, Wu L, Wu L, Dhanjai FuL, Gao Y, Chen J (2016) Response characteristics of bisphenols on a metal-organic framework-based tyrosinase nanosensor. ACS Appl Mater Interfaces 8:16533–16539. https://doi.org/10.1021/ACSAMI.6B05008

Miller JC, Miller JN (1993) Statistics for analytical chemistry, 4th edn. Ellis Horwood PTR Prentice Hall, New York

Mo F, Xie J, Wu T, Liu M, Zhang Y, Yao S (2019) A sensitive electrochemical sensor for bisphenol A on the basis of the AuPd incorporated carboxylic multi-walled carbon nanotubes. Food Chem 292:253–259. https://doi.org/10.1016/J.FOODCHEM.2019.04.034

Narwade SS, Mali SM, Sathe BR (2021) Amine-functionalized multi-walled carbon nanotubes (EDA-MWCNTs) for electrochemical water splitting reactions. New J Chem 45:3932–3939. https://doi.org/10.1039/D0NJ05479H

Noordadi M, Mehrnejad F, Sajedi RH, Jafari M, Ranjbar B (2018) The potential impact of carboxylic-functionalized multi-walled carbon nanotubes on trypsin: a comprehensive spectroscopic and molecular dynamics simulation study. PLoS One 13https://doi.org/10.1371/JOURNAL.PONE.0198519

Pang YH, Huang YY, Wang L, Shen XF, Wang YY (2020) Determination of bisphenol A and bisphenol S by a covalent organic framework electrochemical sensor. Environ Pollut 263:114616. https://doi.org/10.1016/J.ENVPOL.2020.114616

Rao H, Zhao X, Liu X, Zhong J, Zhang Z, Zou P, Jiang Y, Wang X, Wang Y (2018) A novel molecularly imprinted electrochemical sensor based on graphene quantum dots coated on hollow nickel nanospheres with high sensitivity and selectivity for the rapid determination of bisphenol S. Biosens Bioelectron 100:341–347. https://doi.org/10.1016/J.BIOS.2017.09.016

Rocha BA, de Oliveira ARM, Barbosa F (2018) A fast and simple air-assisted liquid-liquid microextraction procedure for the simultaneous determination of bisphenols, parabens, benzophenones, triclosan, and triclocarban in human urine by liquid chromatography-tandem mass spectrometry. Talanta 183:94–101. https://doi.org/10.1016/J.TALANTA.2018.02.052

Schäfer AI, Nghiem LD, Oschmann N (2006) Bisphenol A retention in the direct ultrafiltration of greywater. J Memb Sci 283:233–243. https://doi.org/10.1016/J.MEMSCI.2006.06.035

Shalom M, Gimenez S, Schipper F, Herraiz-Cardona I, Bisquert J, Antonietti M (2014) Controlled carbon nitride growth on surfaces for hydrogen evolution electrodes. Angew Chemie Int Ed 53:3654–3658. https://doi.org/10.1002/ANIE.201309415

Smith REG, Davies TJ, Baynes NDB, Nichols RJ (2015) The electrochemical characterisation of graphite felts. J Electroanal Chem 747:29–38. https://doi.org/10.1016/J.JELECHEM.2015.03.029

Thoene M, Rytel L, Nowicka N, Wojtkiewicz J (2018) The state of bisphenol research in the lesser developed countries of the EU: a mini-review. Toxicol Res (camb) 7:371. https://doi.org/10.1039/C8TX00064F

Vatanpour V, Haghighat N (2019) Improvement of polyvinyl chloride nanofiltration membranes by incorporation of multiwalled carbon nanotubes modified with triethylenetetramine to use in treatment of dye wastewater. J Environ Manage 242:90–97. https://doi.org/10.1016/J.JENVMAN.2019.04.060

Wang J (2006) Analytical electrochemistry. John Wiley and Sons, Hoboken, New Jersey., Third Edit

Wang X, Lu X, Wu L, Chen J (2015) 3D metal-organic framework as highly efficient biosensing platform for ultrasensitive and rapid detection of bisphenol A. Biosens Bioelectron 65:295–301. https://doi.org/10.1016/J.BIOS.2014.10.010

Wang Q, Zhang D, Yang L, Zhang L (2017) Constructed ILs@ hollow porous spherical Ni-loaded $CdFe_2O_4$ modified electrode for highly sensitive simultaneous electrochemical analysis of bisphenols. Sens Actuators B Chem 246:800–808. https://doi.org/10.1016/J.SNB.2017.02.153

Wang X, Li M, Wu M et al (2018) Simultaneous determination of bisphenol A and bisphenol S using multi-walled carbon nanotubes modified electrode. Int J Electrochem Sci 13:11906–11922. https://doi.org/10.20964/2018.12.80

Wolski P, Nieszporek K, Panczyk T (2017) Pegylated and folic acid functionalized carbon nanotubes as pH controlled carriers of doxorubicin. Molecular dynamics analysis of the stability and drug release mechanism. Phys Chem Chem Phys 19:9300–9312. https://doi.org/10.1039/C7CP00702G

Yang Y, Li M, Zhu Z (2019) A novel electrochemical sensor based on carbon nanotubes array for selective detection of dopamine or uric acid. Talanta 201:295–300. https://doi.org/10.1016/J.TALANTA.2019.03.096

Yao J, Chen M, Li N et al (2019) Experimental and theoretical studies of a novel electrochemical sensor based on molecularly imprinted polymer and B, N, F-CQDs/AgNPs for enhanced specific identification and dual signal amplification in highly selective and ultra-trace bisphenol S determination in plastic products. Anal Chim Acta 1066:36–48. https://doi.org/10.1016/J.ACA.2019.03.051

Ye Z, Wang Q, Qiao J et al (2019) Simultaneous detection of bisphenol A and bisphenol S with high sensitivity based on a new electrochemical sensor. J Electroanal Chem 854:113541. https://doi.org/10.1016/J.JELECHEM.2019.113541

Zhang J, Xu X, Chen Z (2018a) A highly sensitive electrochemical sensor for bisphenol A using cetyltrimethylammonium bromide functionalized carbon nanohorn modified electrode. Ionics (kiel) 24:2123–2134. https://doi.org/10.1007/S11581-018-2462-1

Zhang YF, Ren XM, Li YY et al (2018b) Bisphenol A alternatives bisphenol S and bisphenol F interfere with thyroid hormone signaling pathway in vitro and in vivo. Environ Pollut 237:1072–1079. https://doi.org/10.1016/J.ENVPOL.2017.11.027

Zhao C, Xie P, Yong T et al (2018) MALDI-MS imaging reveals asymmetric spatial distribution of lipid metabolites from bisphenol S-induced nephrotoxicity. Anal Chem 90:3196–3204. https://doi.org/10.1021/ACS.ANALCHEM.7B04540

Zheng Y, Jiao Y, Zhu Y et al (2014) Hydrogen evolution by a metal-free electrocatalyst. Nat Commun 5:3783. https://doi.org/10.1038/ncomms4783

Zheng Z, Liu J, Wang M et al (2016) Selective sensing of bisphenol A and bisphenol S on platinum/poly(diallyl dimethyl ammonium chloride)-diamond powder hybrid modified glassy carbon electrode. J Electrochem Soc 163:B192–B199. https://doi.org/10.1149/2.0281606JES

Zheng W, Xiong Z, Li H et al (2018) Electrodeposited Pt@Molecularly imprinted polymer core-shell nanostructure: enhanced sensing platform for sensitive and selective detection of bisphenol A. Sensors Actuators B Chem 272:655–661. https://doi.org/10.1016/J.SNB.2018.07.039

Zhu W, Yue X, Duan J et al (2016) Electrochemically co-reduced 3D GO-C60 nanoassembly as an efficient nanocatalyst for electrochemical detection of bisphenol S. Electrochim Acta 188:85–90. https://doi.org/10.1016/J.ELECTACTA.2015.11.131